Electronic Supplementary Material (ESI) for Nanoscale.

Supporting Information

Fe_3O_4 Nanoplates Anchored on the $Ti_3C_2T_x$ MXene with Enhanced Pseudocapacitive and Electrocatalytic Properties

*Lu Zhang,‡ Zhuo Wang,‡ Wenxiao Chen, Ruiwen Yuan, Ke Zhan, Min Zhu, Junhe Yang, and Bin Zhao**

School of Materials Science and Engineering, University of Shanghai for Science and Technology, Shanghai 200093, China.

Corresponding Author

*E-mail: zhaobin@usst.edu.cn

The Computational equations

According to the equation (1), the gravimetric specific capacitance of an electrode material can be expressed as follow:

$$C_g = \frac{I\Delta t}{m\Delta V} \tag{1}$$

where I is the current density, t is the discharge time, m is the mass of the active material and V is the potential window.

The charge/discharge process is dominated by diffusion or capacitance behavior can be qualitatively analyzed by the following equations:

$$i = ab^{v} \tag{2}$$

$$log\ i = b \times log\ v + log\ a \tag{3}$$

where *i* is the current, *v* is the scan rate and a is a constant. The slope b is obtained by fitting *log i* and *log v*. If the *b* value is close to 0.5, this suggests *a* linear diffusion-controlled process, while values close to 1.0 represent a capacitive-controlled behaviour.

The contribution rate of capacitance at a specific scan rate can be quantitatively calculated by the following equation:

$$i(V) = k_1 v + k_2 v^{1/2} \tag{4}$$

where the capacitive contribution ($k_1 v$) and the linear diffusion-controlled contribution ($k_2 v^{1/2}$).

The overpotential (η) was calculated using the following equation:

$$\eta(V) = E(V\ vs.\ RHE) - 1.23\ V \tag{5}$$

considering O_2/H_2O equilibrium at 1.23 V vs. RHE.

Tafel equation was derived by fitting the linear portion of the tafel plots and the tafel slope was used to evaluate of the OER activities of the investigated catalysts:

$$\eta(V)=b\log(j/j_0) \tag{6}$$

where η is the overpotential, b is the Tafel slope, j is the current density and j_0 is the exchange current density.

Table S1 Phsicochemical parameters of the MXene-Fe composites.

Samples	BET (m^2 g^{-1})	D (nm)	V (cm^3 g^{-1})
MXene-Fe-1	12.2	11.38	0.034
MXene-Fe-2	41.3	6.84	0.104
MXene-Fe-3	61.8	7.74	0.176
MXene-Fe-4	44.8	8.83	0.113

Table S2 Summary of the specific capacitance, overpotential, Tafel slope and C_{dl} for different composites measured in 1.0 M KOH.

Samples	Specific capacitance ($F\ g^{-1}$)	η_{10} (mV)	Tafel slope ($mV\ dec^{-1}$)	C_{dl} ($mF\ cm^{-2}$)
$Ti_3C_2T_x$	46.0	470	71.6	0.35
MXene-Fe-1	170.6	340	68.0	0.735
MXene-Fe-2	289.0	300	65.1	0.785
MXene-Fe-3	368.0	290	76.1	0.86
MXene-Fe-4	172.6	470	133.0	0.795

Table S3. Comparison of supercapacitive performance of the $Ti_3C_2T_x$-Fe composite and the related $Ti_3C_2T_x$-based electrodes in literatures.

Samples	Voltage window	Electrolyte	Specific capacitance	Ref.
$Ti_3C_2T_x$/Fe-3	**-1.1~-0.3 V**	**1 M KOH**	**1 A g^{-1}, 368 F g^{-1}**	**This work**
Ti_3C_2-foam	-1~-0.5 V	1 M KOH	5 mV s^{-1}, 122.7 F g^{-1}	S1
V_2C	-1.1~-0.6 V	1 M KOH	2 mV s^{-1}, 184 F g^{-1}	S2
$Ti_3C_2T_x$	-0.8~0 V	6 M KOH	1 A g^{-1}, 197 F g^{-1}	S3
Fe_3O_4	-0.2~0.25 V	3 M KOH	2 mV s^{-1}, 101 F g^{-1}	S4
MnO_2-Ti_3C_2	-1~-0.4 V	6 M KOH	5 mV s^{-1}, 140 F g^{-1}	S5
PANI@TiO_2/$Ti_3C_2T_x$	-1~-0.3 V	1 M KOH	1 A g^{-1}, 108.9 F g^{-1}	S6
$Ti_3C_2T_x$-Al^{3+}	-1~-0.4 V	1 M KOH	0.3 A g^{-1}, 175 F g^{-1}	S7
PVP-Mn/ak Ti_3C_2 PVP-Ni/ak Ti_3C_2	-1.1~-0.4 V	1 M KOH	0.3 A g^{-1}, 154.6 F g^{-1} 0.3 A g^{-1}, 167.5 F g^{-1}	S8
MoO_3/TiO_2/$Ti_3C_2T_x$	-1~-0.3 V	1 M KOH	2 mV s^{-1}, 162 F g^{-1}	S9

Table S4 The detailed values of impedance in Fig 6c. Rs: resistivity of solution; CPE-T: Constant phase element-T; CPE-P: Constant phase element-P; Rct: resistivity of charge transfer.

Samples	Element	Value
MXene-Fe-1	R_s	1.365
	CPE-T	0.055976
	CPE-P	0.62019
	$\boldsymbol{R_{ct}}$	**18.78**
MXene-Fe-2	R_s	1.39
	CPE-T	0.030362
	CPE-P	0.70702
	$\boldsymbol{R_{ct}}$	**6.624**
MXene-Fe-3	R_s	1.31
	CPE-T	0.081123
	CPE-P	0.55656
	$\boldsymbol{R_{ct}}$	**3.913**
MXene-Fe-4	R_s	1.523
	CPE-T	0.024338
	CPE-P	0.68198
	$\boldsymbol{R_{ct}}$	**24.67**

Table S5 Comparison of OER performance of the $Ti_3C_2T_x$-Fe composite and the related $Ti_3C_2T_x$-based electrocatalyst in literatures.

Samples	η_{10}	Tofel slope (mV dec^{-1})	Electrolyte	Ref.
$Ti_3C_2T_x$-Fe-3	**290 mV**	**65.1**	**1 M KOH**	**This work**
Co-LDH@$Ti_3C_2T_x$	340 mV	82	1 M KOH	S10
NiCoS/$Ti_3C_2T_x$ NiCo -LDH/$Ti_3C_2T_x$	360 mV 480 mV	58 153.1	1 M KOH	S11
$Ti_3C_2T_x$-CoBDC	410 mV	48.2	0.1 M KOH	S12
1T/2H $MoSe_2$/Mxene	340 mV	90	1 M KOH	S13
BP/MXene	360 mV	64.3	1 M KOH	S14
Co^{3+}-$Ti_3C_2T_x$	425 mV	63.5	1 M KOH	S15
Co/N-CNTs@$Ti_3C_2T_x$	411 mV	79.1	0.1 M KOH	S16
CoP@Ti_3C_2	320 mV	59	1 M KOH	S17
CoP/Ti_3C_2 MXene	280 mV	95.4	1 M KOH	S18
CoFe-LDH/MXene	319 mV	50	1 M KOH	S19

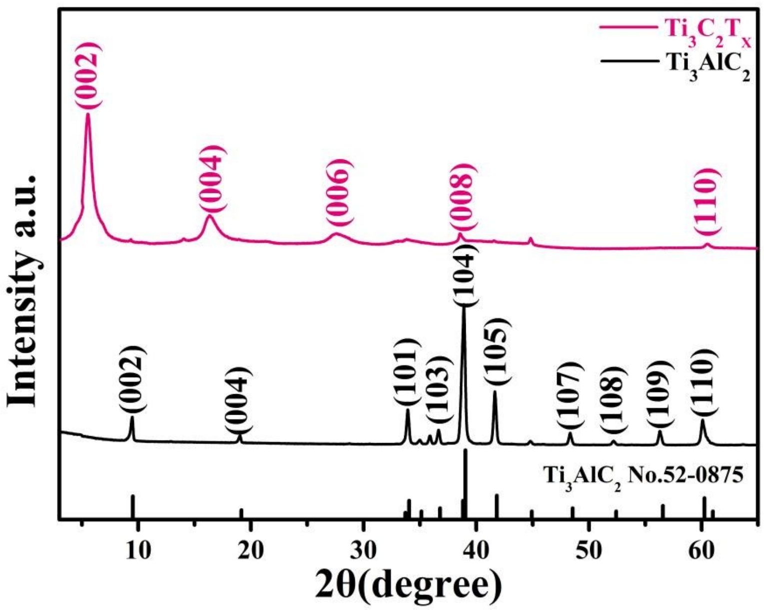

Fig. S1 XRD patterns of Ti_3AlC_2 and $Ti_3C_2T_x$ samples**.**

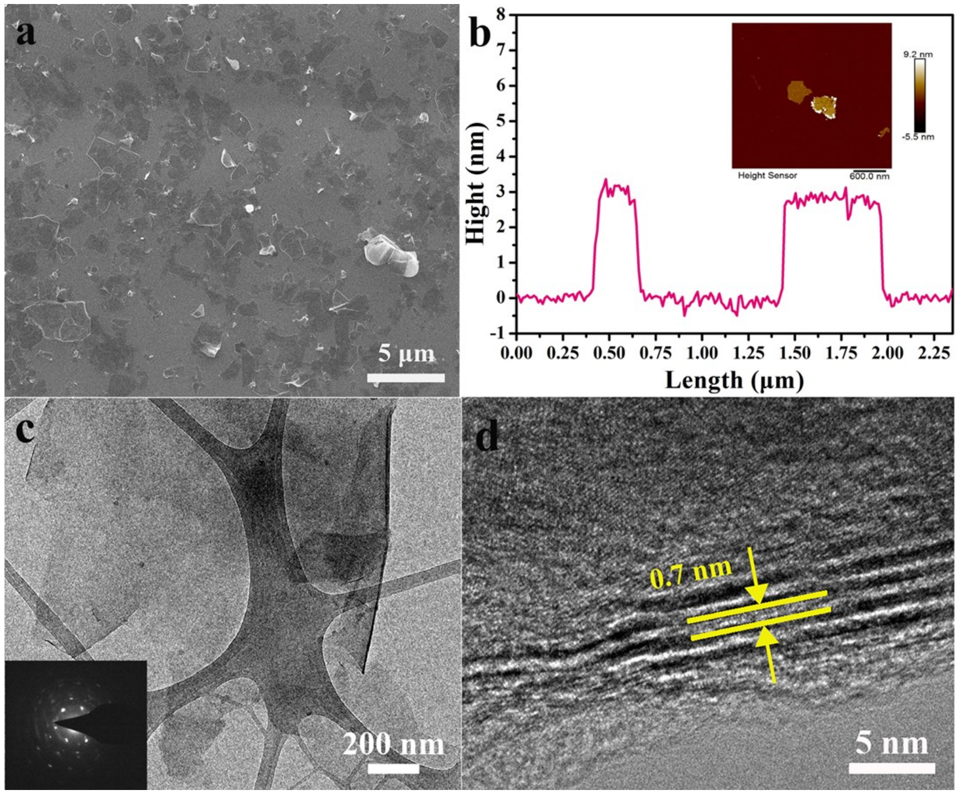

Fig. S2 (a) SEM (b) AFM (c) TEM (the inset shows the corresponding diffraction pattern) and (d) HRTEM images of $Ti_3C_2T_x$ nanosheet with corresponding height profile.

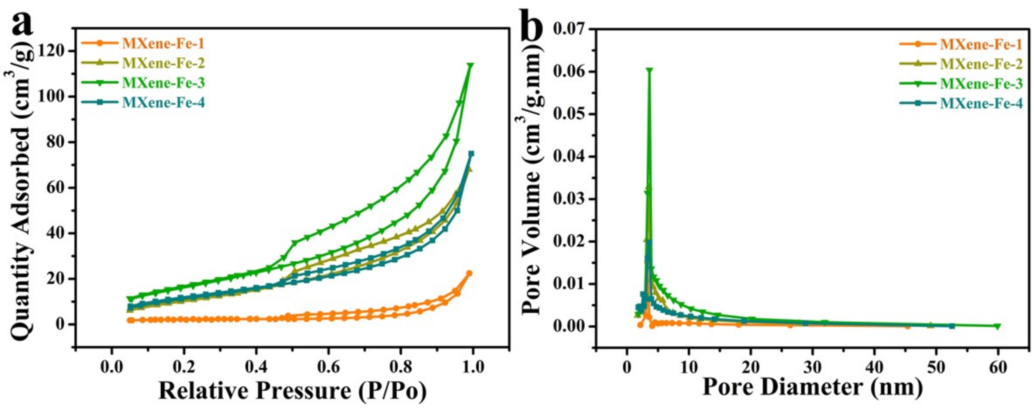

Fig. S3 Nitrogen gas sorption isotherm at 77 K (a) and (b) corresponding pore size distribution of MXene-Fe-1, MXene-Fe-2, MXene-Fe-3 and MXene-Fe-4.

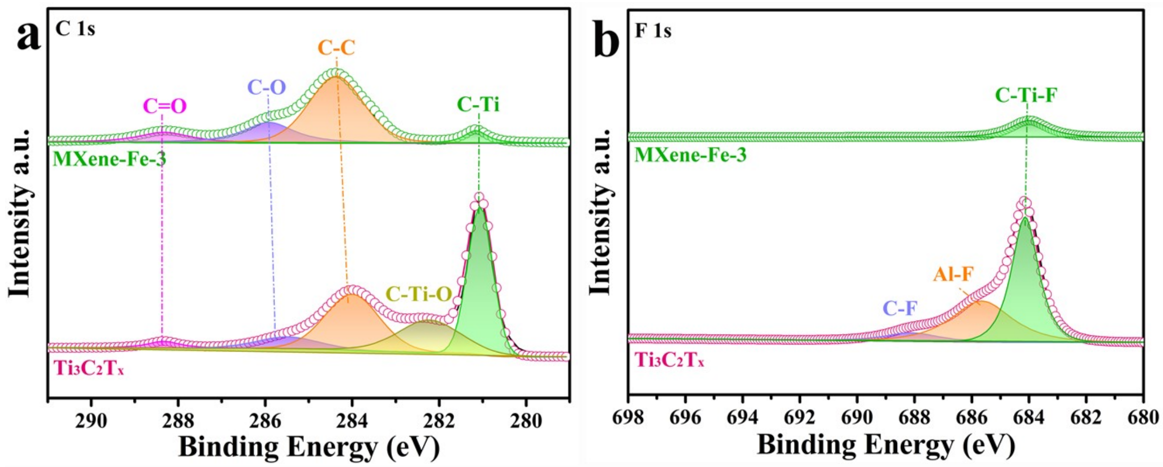

Fig. S4 High-resolution XPS spectra for (a) C 1s, (b) F 1s of $Ti_3C_2T_x$ and MXene-Fe-3 samples, respectively.

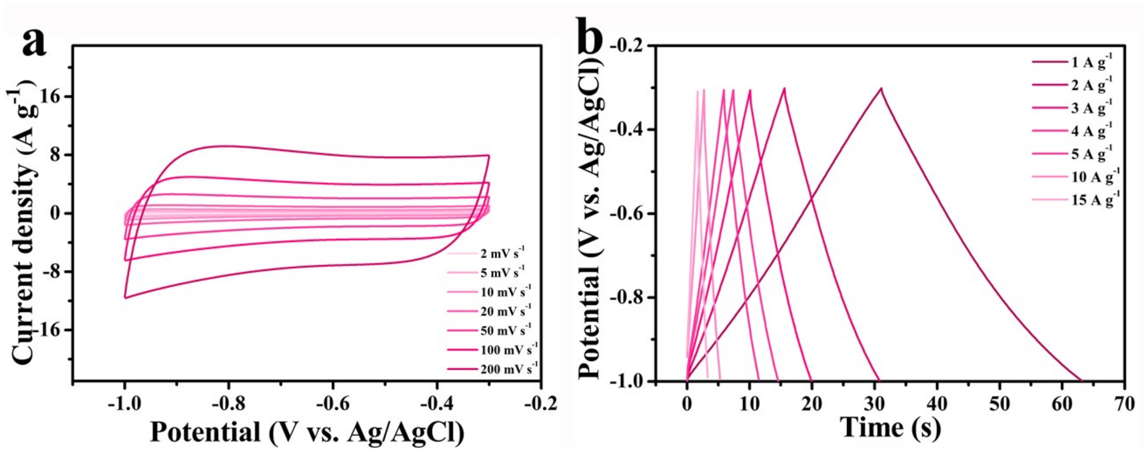

Fig. S5 (a) CV curves of the $Ti_3C_2T_x$ at scan rates of 2 to 200 mV s^{-1} in a potential window of -1.0 ~ -0.3 V. (b) GCD curves of the $Ti_3C_2T_x$ at current densities of 1 to 15 A g^{-1} in a potential window of -1.0 ~ -0.3 V.

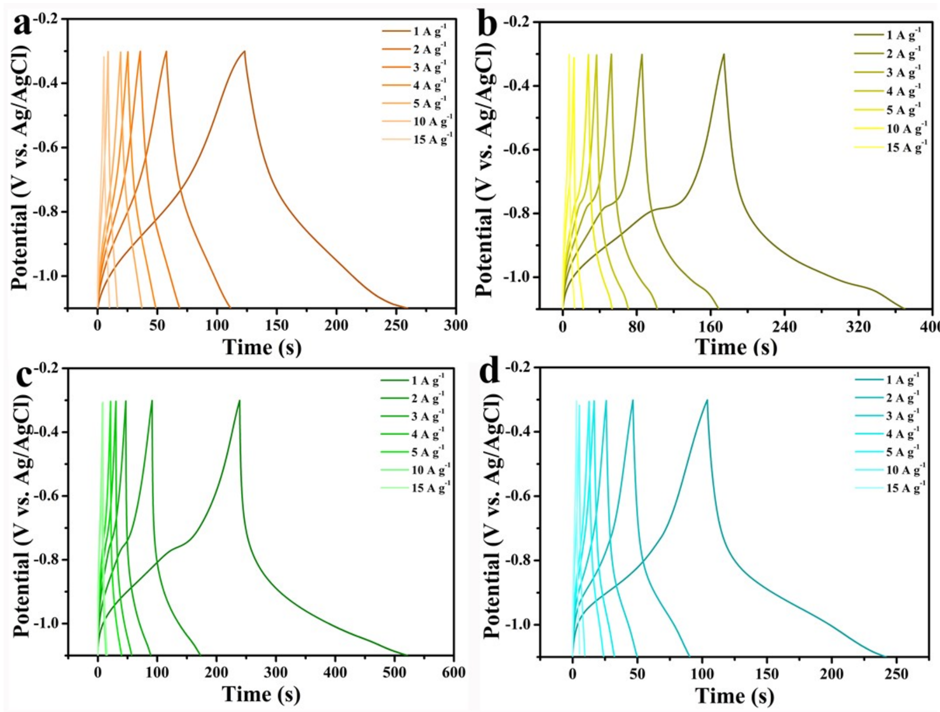

Fig. S6 GCD curves of the (a) MXene-Fe-1, (b) MXene-Fe-2, (c) MXene-Fe-3 and (d) MXene-Fe-4 at current densities of 1 to 15 A g^{-1} in a potential window of -1.1 ~ -0.3 V.

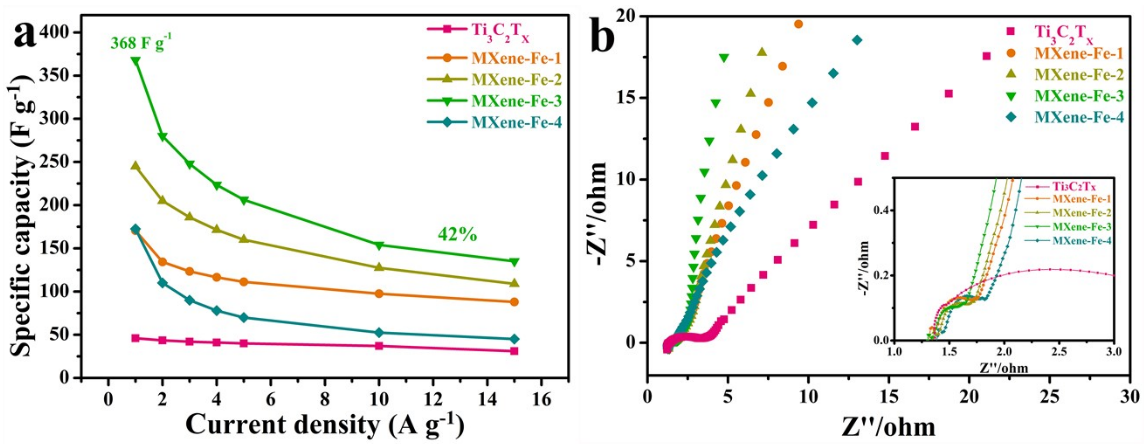

Fig. S7 (a) Specific capacities as a function of discharge current densities calculated from the GCD curves. (b) Nyquist curves of $Ti_3C_2T_x$, MXene-Fe-1, MXene-Fe-2, MXene-Fe-3 and MXene-Fe-4 electrodes, inset showing high-frequency parts of the EIS spectra for these samples.

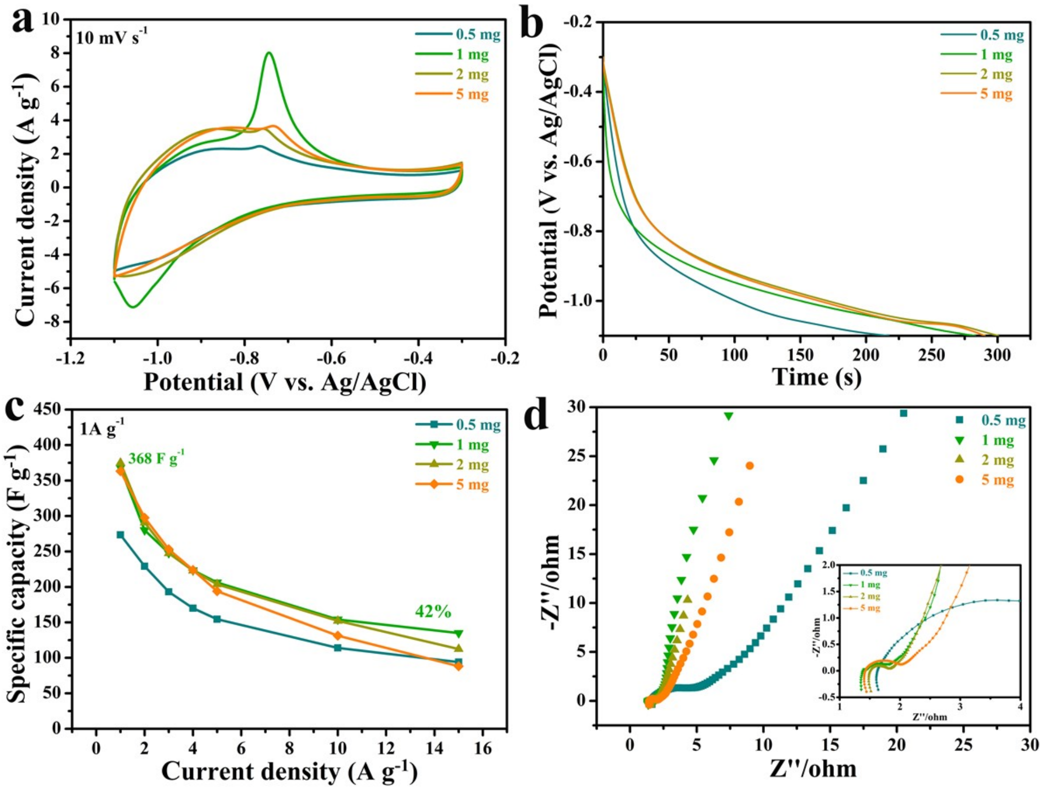

Fig. S8 Electrochemical performance of the MXene-Fe-3 with the different mass of the active substance. (a) CV curves at 10 mV s^{-1} and (b) GCD curves at 1 A g^{-1}, (c) Specific capacities as a function of discharge current densities calculated from the GCD curves and (d) Nyquist curves, inset showing high-frequency parts of the EIS spectra for these samples.

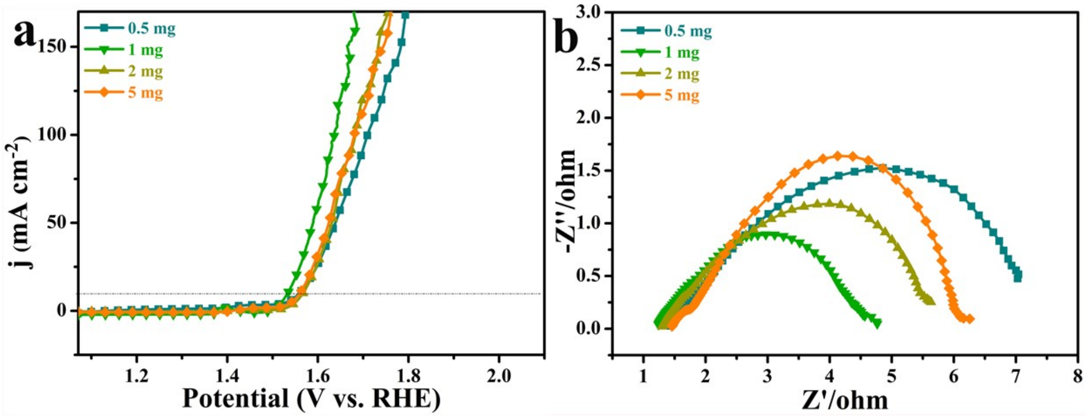

Fig. S9 Electro-catalytic property tests of the MXene-Fe-3 with the different mass of the active substance. (a) LSV curves and (b) Nyquist plots of the above electrodes measured at a potential of 1.50 V vs. RHE.

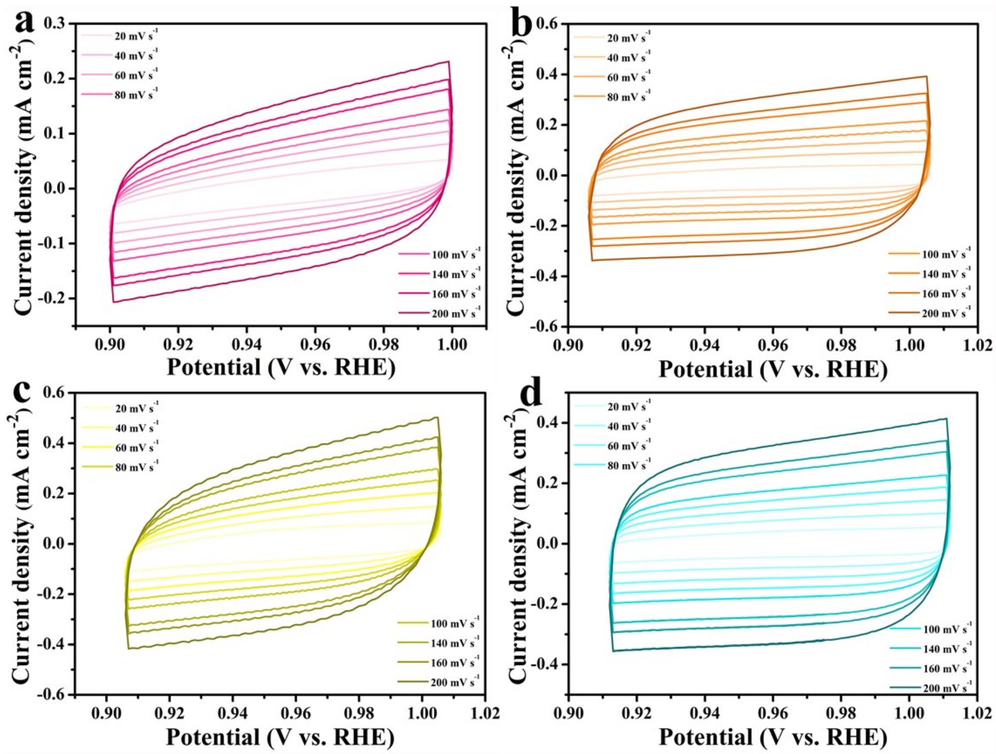

Fig. S10 Cyclic voltammograms (CVs) of (a) $Ti_3C_2T_x$, (b) MXene-Fe-1, (c) MXene-Fe-2, and (d) MXene-Fe-4 at various scan rates.

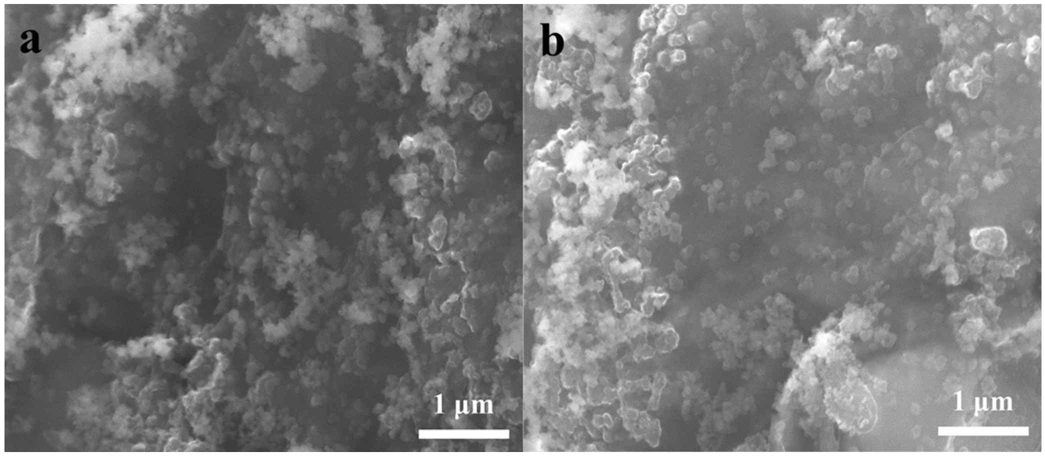

Fig. S11 SEM image of MXene-Fe-3 after OER stability test in 1 M KOH.

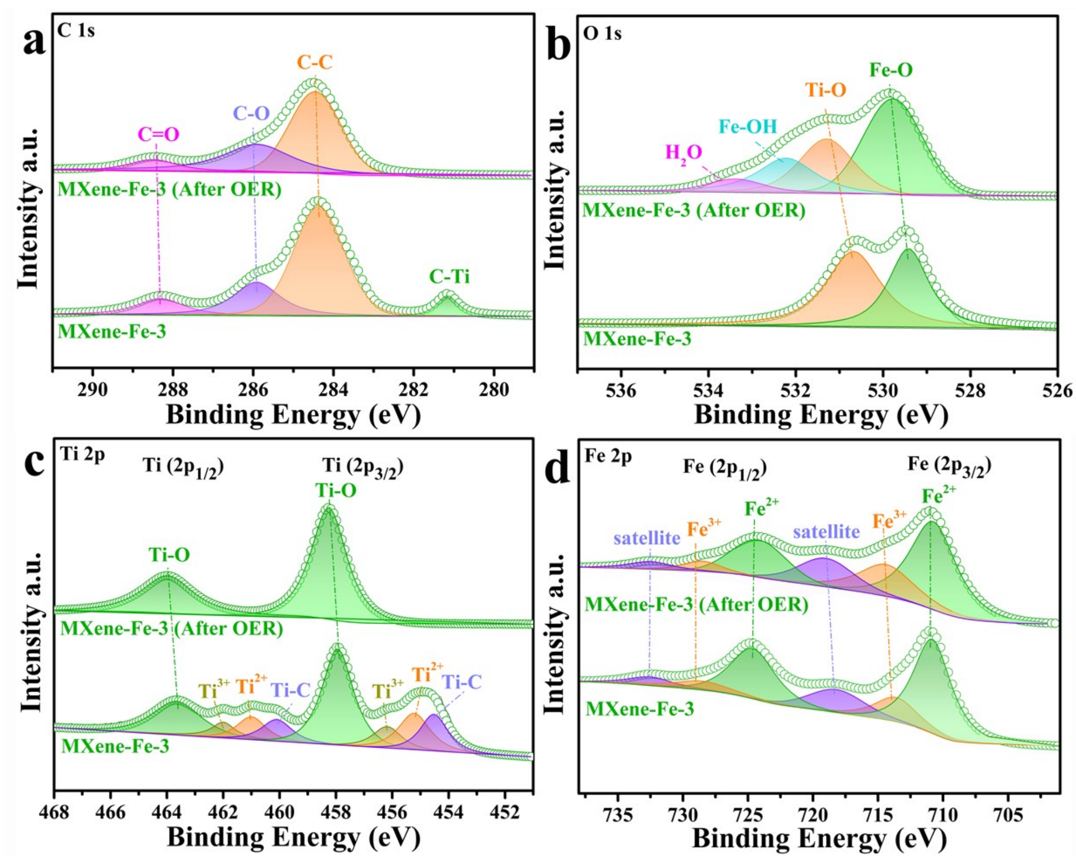

Fig. S12 High resolution XPS spectra of the MXene-Fe-3 before and after OER test: (a) C 1s, (b) O 1s, (c) Ti 2p and (d) Fe 2p.

References

S1 L. Shi, S. Lin, L. Li, W. Wu, L. Wu, H. Gao and X. Zhang, *Ceramics International*, 2018, **44**, 13901-13907.

S2 Q. Shan, X. Mu, M. Alhabeb, C. E. Shuck, D. Pang, X. Zhao, X.-F. Chu, Y. Wei, F. Du, G. Chen, Y. Gogotsi, Y. Gao and Y. Dall'Agnese, *Electrochemistry Communications*, 2018, **96**, 103-107.

S3 S. Venkateshalu and A. N. Grace, *Electrochimica Acta*, 2020, **341**, 136035.

S4 M. L. Aparna, A. N. Grace, P. Sathyanarayanan and N. K. Sahu, *Journal of Alloys and Compounds*, 2018, **745**, 385-395.

S5 Y. Tang, J. Zhu, C. Yang and F. Wang, *Journal of Alloys and Compounds*, 2016, **685**, 194-201.

S6 X. Lu, J. Zhu, W. Wu and B. Zhang, *Electrochimica Acta*, 2017, **228**, 282-289.

S7 Y. Li, Y. Deng, J. Zhang, Y. Han, W. Zhang, X. Yang, X. Zhang and W. Jiang, *Nanoscale*, 2019, **11**, 21981-21989.

S8 W. Zhang, J. Zhang, Y. Li and X. Yang, *Ceramics International*, 2020, **46**, 15492-15501.

S9 Q. Zhao, J. Zhu, X. Lu, W. Zhou and X. Li, *Journal of Alloys and Compounds*, 2018, **767**, 264-269.

S10 M. Benchakar, T. Bilyk, C. Garnero, L. Loupias, C. Morais, J. Pacaud, C. Canaff, P. Chartier, S. Morisset, N. Guignard, V. Mauchamp, S. Célérier and A. Habrioux, *Advanced Materials Interfaces*, 2019, **6**, 1901328.

S11 H. Zou, B. He, P. Kuang, J. Yu and K. Fan, *ACS applied materials & interfaces*, 2018, **10**, 22311-22319.

S12 L. Zhao, B. Dong, S. Li, L. Zhou, L. Lai, Z. Wang, S. Zhao, M. Han, K. Gao, M. Lu, X. Xie, B. Chen, Z. Liu, X. Wang, H. Zhang, H. Li, J. Liu, H. Zhang, X. Huang and W. Huang, *ACS nano*, 2017, **11**, 5800-5807.

S13 N. Li, Y. Zhang, M. Jia, X. Lv, X. Li, R. Li, X. Ding, Y.-Z. Zheng and X. Tao, *Electrochimica Acta*, 2019, **326**, 134976.

S14 X.-D. Zhu, Y. Xie and Y.-T. Liu, *Journal of Materials Chemistry A*, 2018, **6**, 21255-21260.

S15 S. Y. Pang, Y. T. Wong, S. Yuan, Y. Liu, M. K. Tsang, Z. Yang, H. Huang, W. T. Wong and J. Hao, *Journal of the American Chemical Society*, 2019, **141**, 9610-9616.

S16 Y. Zhang, H. Jiang, Y. Lin, H. Liu, Q. He, C. Wu, T. Duan and L. Song, *Advanced Materials Interfaces*, 2018, **5**, 1800392.

S17 L. Yan, B. Zhang, S. Wu and J. Yu, *Journal of Materials Chemistry A*, 2020, **8**, 14234-14242.

S18 L. Xiu, Z. Wang, M. Yu, X. Wu and J. Qiu, *ACS nano*, 2018, **12**, 8017-8028.

S19 C. Hao, Y. Wu, Y. An, B. Cui, J. Lin, X. Li, D. Wang, M. Jiang, Z. Cheng and S. Hu, *Materials Today Energy*, 2019, **12**, 453-462.